J. Fluid Mech. (2014), *vol.* 758, R3, doi:10.1017/jfm.2014.539

JFM RAPIDS
journals.cambridge.org/rapids

Undulatory swimming in shear-thinning fluids: experiments with *Caenorhabditis elegans*

D. A. Gagnon[1], N. C. Keim[1] and P. E. Arratia[1,†]

[1]Department of Mechanical Engineering and Applied Mechanics, University of Pennsylvania, Philadelphia, PA 19104, USA

(Received 21 July 2014; revised 13 September 2014; accepted 14 September 2014; first published online 7 October 2014)

The swimming behaviour of micro-organisms can be strongly influenced by the rheology of their fluid environment. In this article, we experimentally investigate the effects of shear-thinning (ST) viscosity on the swimming behaviour of an undulatory swimmer, the nematode *Caenorhabditis elegans*. Tracking methods are used to measure the swimmer's kinematic data (including propulsion speed) and velocity fields. We find that ST viscosity modifies the velocity fields produced by the swimming nematode but does not modify the nematode's speed and beating kinematics. Velocimetry data show significant enhancement in local vorticity and circulation and an increase in fluid velocity near the nematode's tail. These findings are compared with recent theoretical and numerical results.

Key words: complex fluids, micro-organism dynamics, swimming/flying

1. Introduction

Swimming organisms, such as sperm cells (Fauci & Dillon 2006), bacteria and many types of protozoa (Lauga & Goldstein 2012), and multicellular organisms (Sznitman *et al.* 2010*a*), are essential components of numerous biological processes, from reproduction in mammals (Fauci & Dillon 2006) and infections such as Lyme disease (Harman *et al.* 2012) to biodegradation in soil (Alexander 1991). Due to their small length scales ($L \lesssim 1$ mm), the abovementioned organisms live in low-Reynolds-number regimes ($Re \ll 1$) where linear viscous forces are much larger than nonlinear forces from inertia. At low Re, locomotion requires non-reciprocal deformations to break time-reversal symmetry, which is commonly referred to as the 'scallop theorem' (Purcell 1977).

Recently, a number of studies have focused on understanding the swimming behaviour of micro-organisms at low Re in simple Newtonian fluids (Lauga & Powers 2009; Guasto, Johnson & Gollub 2010; Lauga & Goldstein 2012; Saintillan & Shelley 2012). However, many organisms swim in non-Newtonian environments

† Email address for correspondence: parratia@seas.upenn.edu

such as mucus, blood and soil (Alexander 1991; Harman *et al.* 2012) that often exhibit viscoelasticity and shear-rate-dependent viscosity. While much work has been devoted to the effects of fluid elasticity on the swimming of micro-organisms (Lauga 2007; Fu, Wolgemuth & Powers 2009; Fu, Shenoy & Powers 2010; Teran, Fauci & Shelley 2010; Liu, Powers & Breuer 2011; Shen & Arratia 2011), there are relatively few studies of swimming in shear-thinning (ST) fluids.

To date, major studies of the effects of ST viscosity are theoretical (Vélez-Cordero & Lauga 2013) and numerical (Montenegro-Johnson *et al.* 2012; Montenegro-Johnson, Smith & Loghin 2013). The theoretical analysis focuses on a two-dimensional infinite waving sheet immersed in a model Carreau (ST) fluid, and finds a non-Newtonian contribution to propulsion speed to fourth order in amplitude when the sheet is extensible. However, no non-Newtonian contribution to propulsion speed is found when an inextensible condition is applied (Vélez-Cordero & Lauga 2013). Additionally, for a finite swimmer, this analysis suggests that the cost of transport is reduced and the flow field is modified by ST fluids, resulting in increased vorticity near the sheet (Vélez-Cordero & Lauga 2013). Separate simulations (Montenegro-Johnson *et al.* 2012, 2013) also using the Carreau model suggest that undulatory swimmers with a head or 'payload' (similar to a sperm cell) are assisted by ST viscosity, resulting in increased speed, and that the swimmer's motion results in an envelope of thinned fluid around the body.

Despite these recent and important efforts, there is still a dearth of experimental investigations of swimming in ST fluids, and the effects of rate-dependent viscosity on swimming remain unclear. Experiments with a mechanical model system (Dasgupta *et al.* 2013) find a decrease in propulsion for fluids possessing both ST and viscoelastic behaviour. Additionally, the swimming speed of *Caenorhabditis elegans* is shown to be unaffected by ST viscosity (Shen & Arratia 2011), although only a single data point is available.

Here, we experimentally investigate the effects of ST viscosity on the swimming behaviour of a model biological organism, the nematode *C. elegans*. The nematode's position and swimming stroke are tracked using in-house software (Sznitman *et al.* 2010*b*) and flow fields are obtained using particle tracking methods (Sznitman *et al.* 2010*a*). The results show that there is no change in the nematode's kinematics due to ST effects. However, with this unchanged swimming stroke, the nematode in ST fluid generates a remarkably different flow field, with enhanced vorticity and an altered spatial pattern of fluid velocity. We compare these experimental results with recent analysis (Vélez-Cordero & Lauga 2013) and numerical simulations (Montenegro-Johnson *et al.* 2012, 2013).

2. Experimental methods

The swimming behaviour of the nematode *C. elegans* in ST fluids is investigated in a sealed acrylic chamber that is 2 cm in diameter and 1 mm in depth (figure 1*a*) using a microscope and a high-speed camera. *C. elegans* is a roundworm widely used for biological research (Rankin 2002), which swims by generating travelling waves (Sznitman *et al.* 2010*a*); the organisms are approximately 1 mm in length and 80 μm in diameter. Two main types of experiments are performed: (i) tracer particle velocimetry, used to obtain velocity fields, and (ii) nematode tracking, used to obtain kinematic data such as swimming speed, beating frequency and amplitude. Images are recorded with the focal plane at the centre of the chamber to avoid movies with nematode–wall interactions; out-of-plane recordings are discarded. The kinematics data are an average of at least 15 recordings in each fluid tested.

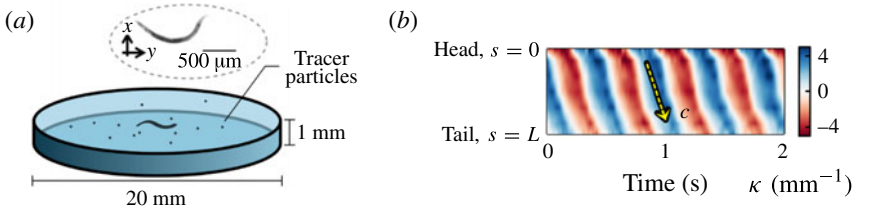

FIGURE 1. (*a*) Schematic of the nematode *C. elegans* swimming in a sealed fluidic chamber. Inset: sample image. (*b*) The nematode's body curvature during swimming. The curvature plot for approximately four beating cycles illustrates a characteristic travelling wave propagating from head to tail. The wave speed c is highlighted by the yellow dashed arrow.

The nematode's swimming kinematics are obtained from videos using in-house software (Sznitman *et al.* 2010*b*). The software measures the nematode's centroid position and body contour, and computes quantities such as swimming speed U and body curvature κ. The swimming speed is obtained by differentiating the nematode's centroid position with time, and we define the positive y-axis as the swimming direction (see figure 1*a*). The body curvature is defined as $\kappa = \delta\phi/\delta s$, where ϕ is the angle between a fixed reference axis and the tangent to the body contour, at each point of an arclength parameterization s along the body contour. Figure 1(*b*) shows the evolution of $\kappa(s, t)$ for approximately four beating cycles, revealing periodic lines that propagate in time from head ($s = 0$) to tail ($s = L$), illustrating the characteristic travelling wave of undulatory swimming. The slope and rate of occurrence of these lines represent the wave speed c (figure 1*b*, yellow dashed line) and beating frequency f, respectively. In water-like buffer solutions, we find $U \approx 0.35$ mm s^{-1}, $f \approx 2$ Hz and $c \approx 5$ mm s^{-1}. The Reynolds number, defined as $Re = \rho UL/\eta$, is approximately 0.35, where L is the nematode's length (1 mm), ρ is the fluid's density (10^3 kg m^{-3}) and η is the fluid's viscosity (1 mPa s), indicating that viscous forces dominate the flow. The range of Reynolds numbers for all experiments is $10^{-4} < Re \leqslant 0.35$.

The Newtonian fluids of various viscosities are (i) a water-like buffer solution (M9 salt solution (Brenner 1974), $\eta = 1$ mPa s), (ii) very dilute solutions of the polymer carboxymethyl cellulose (CMC, 7×10^5 MW, Sigma Aldrich 419338) in M9 salt solution ($2 \leqslant \eta \leqslant 12$ mPa s) and (iii) mixtures of halocarbon oils (Sigma Aldrich H8773 and H8898, $27 \leqslant \eta \leqslant 700$ mPa s). From among these fluids, we can obtain (Newtonian) viscosities ranging from 1 to 700 mPa s. We note that while aqueous solutions of CMC can exhibit viscoelasticity (CMC is a flexible polymer), one can drastically minimize the elasticity of such solutions by using low polymer concentrations and salt in solution. Under these conditions (low CMC concentration and presence of salt) CMC solutions exhibit Newtonian viscosity behaviour and negligible elasticity.

The ST fluids are dilute aqueous solutions of the stiff 'rod-like' polymer xanthan gum (XG) in M9 buffer (XG, 2.7×10^6 MW, Sigma Aldrich G1253). Xanthan gum solutions are known to be ST, with negligible elasticity (Wyatt & Liberatore 2009; Shen & Arratia 2011). We control the strength of ST by varying the XG concentration in solution from 50 to 3000 ppm. The fluids are characterized using a stress-controlled cone-plate rheometer. Figure 2(*a*) shows the shear viscosity as a function of the shear rate for all XG solutions; Newtonian fluids are not shown. Strong ST viscosity is found for the highest-concentration solutions (1000, 2000 and 3000 ppm), while nearly

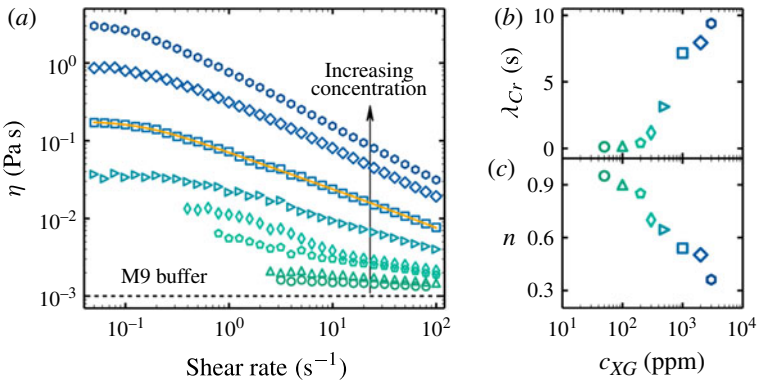

FIGURE 2. (*a*) The shear viscosity of mixtures of XG in M9 buffer solution from 50 to 3000 ppm, which show behaviour characteristic of Carreau–Yasuda model fluids. The dashed line indicates the viscosity of the solvent (M9). The orange line shows a sample fit to the Carreau model. (*b*) The Carreau time scale λ_{Cr} and (*c*) the ST index n calculated using a least-squares fit to the shear viscosity data (see the fitting line in (*a*)).

water-like viscosity is found for the lowest-concentration solutions (50 and 100 ppm). The viscosity data are fitted to the Carreau–Yasuda model (Carreau, DeKee & Chhabra 1997), defined as $\eta(\dot{\gamma}) = \eta_\infty + (\eta_0 - \eta_\infty)(1 + (\lambda_{Cr}\dot{\gamma})^2)^{(n-1)/2}$, where $\eta(\dot{\gamma})$ is the fluid's shear-rate-dependent viscosity, η_0 is the zero-shear viscosity, η_∞ is the infinite-shear viscosity and n is the power-law index. The characteristic time scale λ_{Cr} is the inverse of the shear rate at which the fluid transitions from Newtonian-like to power-law behaviour; it is also the time scale for ST effects to develop or fade away when $\dot{\gamma}$ is changed (Carreau *et al.* 1997).

Figure 2(*b*,*c*) show λ_{Cr} and n as a function of the polymer concentration c_{XG}. As c_{XG} increases, the rise in λ_{Cr} indicates that the fluid requires a lower shear rate to access the ST regime. The power-law index n simultaneously decreases, indicating that the fluid becomes more ST. It should be noted that the power in the Carreau–Yasuda model is defined as $(n-1)/2$; hence a decrease in n means an increase in ST behaviour. The Carreau number $Cr = \lambda_{Cr}\dot{\gamma}$ indicates the degree to which a flow is ST: if $Cr < 1$, the viscosity is Newtonian-like; if $Cr > 1$, the viscosity is ST (Carreau *et al.* 1997).

3. Swimming kinematics

We begin by investigating the swimming kinematics of nematodes in Newtonian and ST fluids. Figure 3(*a–f*) show the nematode's (*a*) swimming speed U, (*b*) beating frequency f, (*c*) beating amplitude A, (*d*) wave speed c, (*e*) Strouhal number $St = fA/U$ and (*f*) kinematic efficiency U/c as a function of the effective viscosity η_{eff} for both Newtonian and ST fluids. It should be noted that for ST fluids, η_{eff} is defined as the average viscosity over a characteristic range of shear rates, $U/L \leqslant \dot{\gamma} \leqslant 2fA/d$. The rate $U/L \approx 0.35\ \mathrm{s}^{-1}$ describes the forward progress of the entire nematode and the rate $2fA/d \approx 15\ \mathrm{s}^{-1}$ describes the nematode's local transverse motion, where $d/2 \approx 40\ \mu\mathrm{m}$ is the body radius. These estimates are in good agreement with measured shear rates.

The data in figure 3 show that the nematode's swimming kinematics in ST fluids are very similar to those in Newtonian fluids of the same effective viscosity. This suggests that the nematode's kinematics are responding solely to bulk viscous effects

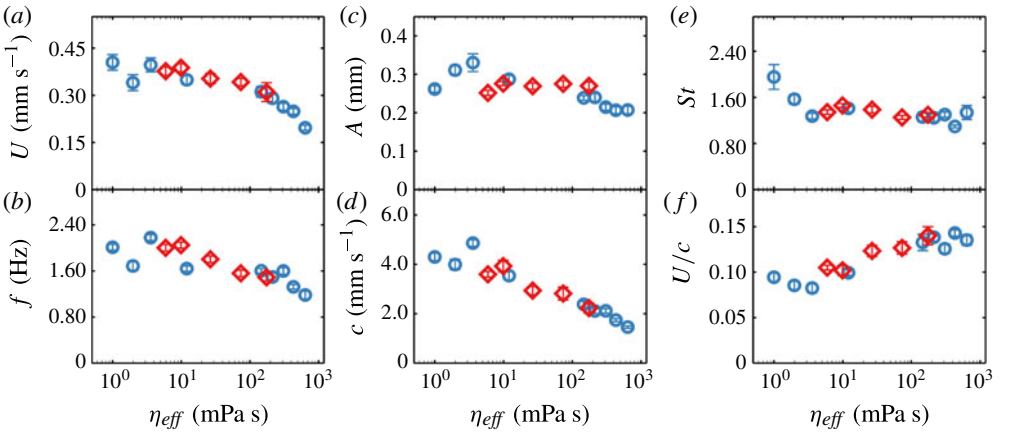

FIGURE 3. Summary of nematode kinematics for Newtonian (○) and ST (◇) fluids. (*a*) Swimming speed U, (*b*) frequency f, (*c*) head amplitude A, (*d*) wave speed c, (*e*) Strouhal number St and (*f*) kinematic efficiency U/c as a function of the effective viscosity η_{eff}. Each data point represents the mean and standard error of approximately 15 recordings.

and not local ST effects. For example, the nematode's swimming speed U (figure 3*a*) is approximately constant for both ST and Newtonian fluids up to $\eta_{eff} \approx 50$ mPa s. A decrease in U is also found for both ST and Newtonian fluids for $\eta_{eff} > 50$ mPa s, which is in agreement with the power-limited nature of *C. elegans* (Shen & Arratia 2011).

Overall, we find no evidence that shear-rate-dependent viscosity influences the swimming stroke or speed of *C. elegans*. Our findings seem to be in agreement, at least in part, with a recent theoretical work (Vélez-Cordero & Lauga 2013), in which the authors find no ST-induced changes to swimming speed for an inextensible sheet. For an extensible sheet, the same study finds an increase in swimming speed in ST fluids. We note, however, that there are differences between our experimental system and the aforementioned theoretical study. For example, the nematode is of finite length and swims using large-amplitude waves that decay from head to tail, while the theoretical work focuses on an infinite two-dimensional waving sheet of prescribed small-amplitude kinematics. Thus, quantitative agreement is not expected.

This theoretical work also proposed a reduction in the cost of transport in an ST fluid. At low Re, power scales as $P \sim \eta V^2$; for swimmers with identical kinematics (same V near the body) and similar effective shear viscosities η_{eff}, we expect P and therefore the cost of transport to be similar. We note that this is just an approximation and a more rigorous calculation using spatially resolved velocity fields (near the nematode's body) and a constitutive model for the ST fluid is necessary (Sznitman *et al.* 2010*a*).

We can also compare our findings with numerical simulations (Montenegro-Johnson *et al.* 2012, 2013) that have predicted an enhancement in swimming speed. The enhancement predicted by this study is for a swimmer with an elliptical head and a linearly increasing amplitude from head to tail; since *C. elegans* has no 'head' and conversely has a decreasing amplitude from head to tail, these differences in geometry and stroke may explain the discrepancy between the predictions of these simulations and our experimental measurements (Montenegro-Johnson *et al.* 2012, 2013).

4. Velocimetry, flow fields and streamlines

In the preceding section, we showed that the swimming strokes of nematodes in ST and Newtonian fluids are quite similar (if not identical). However, the same kinematics may generate different velocity fields. Since the swimming stroke corresponds to the imposed fluid boundary conditions, in Newtonian fluids we expect the flow fields to have a common morphology, with velocity magnitudes merely scaling with viscosity. However, under the same boundary conditions, a non-Newtonian constitutive relation might result in measurable changes to the flow fields. To investigate this possibility, we use particle tracking to measure the flow fields around swimming *C. elegans* in ST and Newtonian fluids. We seed the fluids with 3.1 μm-diameter fluorescent polystyrene spheres, which are tracked in space and time (Sznitman *et al.* 2010*a*; Gagnon, Shen & Arratia 2013). The particles are very dilute (<0.5 % by volume) and do not alter the fluid rheology.

Because the nematode's swimming gait is periodic (figure 1*b*), we can significantly increase the spatial resolution of our flow field measurements by using a phase averaging scheme. We condense multiple beating cycles into a single 'master' cycle by matching frames with the same curvature profile $\kappa(s, t)$, using a least-squares algorithm. This master cycle comprises body shapes and velocity fields at approximately 65 different phases. For more details on this technique, see Sznitman *et al.* (2010*a*).

Figure 4 shows time-averaged velocity magnitude fields in (*a*) buffer solution (Newtonian), (*b*) 200 ppm XG solution and (*c*) 1000 ppm XG solution over one beating cycle. Two features are immediately obvious. First, the regions of high velocity (dark colour) at the nematode's midsection seem to change and intensify as XG concentration and ST effects are increased. Second, there is an overall decrease in average velocity near the head and an increase near the tail as XG concentration increases. These data show that the velocity fields generated by swimming nematodes can be modified by ST effects, even if the imposed swimming kinematics remain unchanged.

To better examine ST effects on the velocity fields, we focus on one particular phase of the beating cycle. While we expect ST effects at every phase, we examine the phase with the largest average shear rate, since this snapshot should reveal the most pronounced differences between Newtonian and ST fluids. Figure 5 shows the velocity magnitude at one phase in (*a*) M9 buffer solution and (*b*) 1000 ppm XG solution. To reduce noise and compensate for differences in bulk viscosity, we normalize the snapshots by their maximum velocity magnitudes: $\hat{v} = |\boldsymbol{v}|/|\boldsymbol{v}|_{max}$; it should be noted that $|\boldsymbol{v}|_{max}$ is similar among fluids (figure 4). Lastly, we subtract the normalized Newtonian field from the normalized ST field; this difference, $\Delta\hat{v} = \hat{v}_{ST} - \hat{v}_N$, is shown in figure 5(*c*). We again find an increase in velocity near the tail and a decrease in velocity near the head.

Figure 5(*c*) also reveals a stark difference near the midsection of the worm, as highlighted by the positive region that begins just below the nematode's head and extends to the right, away from the swimmer. The Newtonian fluid velocity in this region is nearly zero, but for the ST case, this region is part of a large high-velocity lobe. This same region is the site of differences in the fluid streamlines (figure 5*d*,*e*) for the Newtonian and ST cases. The streamlines suggest that in the ST case, the characteristic 'head' and 'tail' vortices have shifted towards the head and are more concentrated. The difference in velocity magnitudes near the midsection is located near the centre of the head vortex, suggesting a potential way to quantify ST effects.

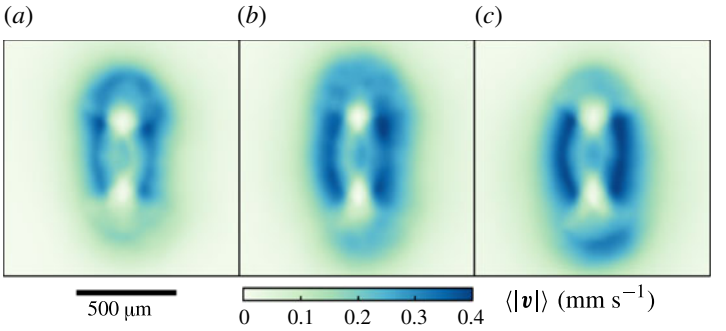

FIGURE 4. (*a–c*) Time-averaged fluid velocity magnitude for one beating cycle of *C. elegans* in (*a*) Newtonian buffer solution, (*b*) ST 200 ppm XG solution and (*c*) ST 1000 ppm XG solution.

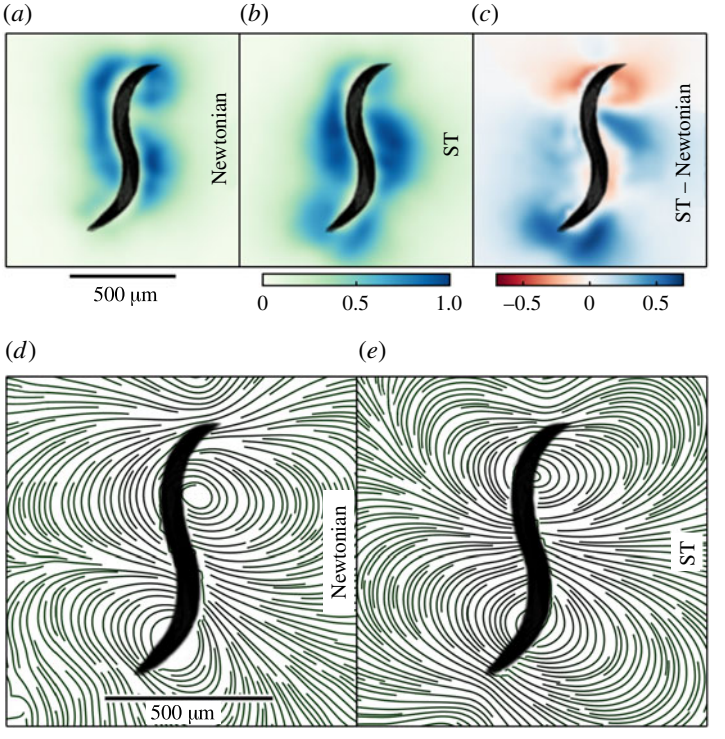

FIGURE 5. (*a*,*b*) Normalized snapshots of velocity magnitude (*a*) $\hat{v}_N$ for a Newtonian fluid ($\eta = 1$ mPa s, $\lambda_{Cr} = 0$ s, $n = 1$) and (*b*) $\hat{v}_{ST}$ for a ST fluid ($\eta_{eff} \approx 11$ mPa s, $\lambda_{Cr} \approx 7$ s, $n \approx 0.5$). (*c*) Snapshot of their difference $\Delta\hat{v} = \hat{v}_{ST} - \hat{v}_N$. (*d*,*e*) Streamlines computed for the same phase for (*d*) Newtonian and (*e*) ST fluids.

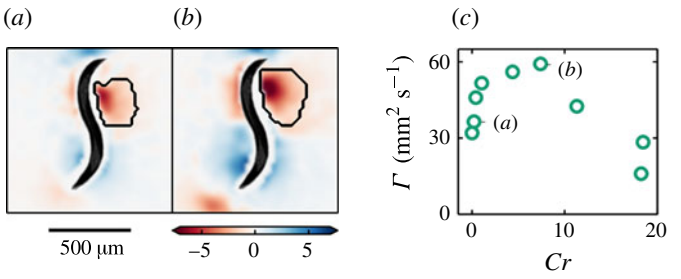

FIGURE 6. Vorticity map calculated for *C. elegans* swimming in (*a*) 50 ppm XG in M9 and (*b*) 500 ppm XG in M9. The region of the head vortex (outlined in black) is defined as the region with vorticity greater than 10 % of the local maximum. (*c*) Circulation Γ of the head vortex for M9 and ST fluids as a function of the expected local importance of shear thinning, $Cr = \lambda_{Cr}\bar{\dot{\gamma}}$, where λ_{Cr} is the Carreau time scale and $\bar{\dot{\gamma}}$ is the measured average local shear rate.

5. Quantifying the role of shear thinning

So far we have shown that ST viscosity has negligible effect on the nematode's swimming kinematics (figure 3) but it does seem to affect the velocity fields generated by swimming (figure 5). Here, we quantify those effects and seek to connect them with the fluids' ST rheology. We begin by inspecting the flow structure (vortex) near the nematode's head for both the Newtonian and ST fluids (figure 5*d*,*e*). For each fluid, we take the velocity field at the same phase as in figure 5, sampled at a grid of points spaced 21 μm apart. We compute the vorticity $\boldsymbol{w}$ in two dimensions, so that $w_z \equiv \partial v_y/\partial x - \partial v_x/\partial y$.

Figure 6(*a*,*b*) show vorticity fields for the 50 and 500 ppm XG solutions, respectively, with the head vortices outlined; it should be noted that the 50 ppm XG vorticity map is not substantially different from the Newtonian case (not shown). We define the head vortex as the region near the head with $|\boldsymbol{w}|$ greater than 10 % of the local maximum. The head vortex is in fact the region of highest vorticity over the entire flow field. The two vorticity fields suggest that increasing the concentration of XG, and thus the ST behaviour of the fluid, increases the magnitude and size of the head vortex. We note that this is not simply due to a change in bulk or 'average' viscosity, since increasing viscosity would merely scale the vorticity field without changing its shape.

Next, we measure the circulation or vorticity flux Γ, which can be thought of as the total vorticity normal to the surface of interest. We compute Γ as the discrete integral of vorticity $w_{z,i}$ at each grid cell i within the vortex region: $\Gamma = \sum a w_{z,i}$, where a is the area of a grid cell. We also use the velocity field and fluid rheology to estimate the expected importance of ST behaviour in the vortex region. This is quantified with a Carreau number $Cr = \lambda_{Cr}\bar{\dot{\gamma}}$. The characteristic vortex shear rate $\bar{\dot{\gamma}}$ is the root-mean-squared (RMS) average over all grid cells in the vortex, where each cell's local shear rate is computed as $\dot{\gamma} \equiv \partial v_x/\partial y + \partial v_y/\partial x$.

Figure 6(*c*) summarizes our measurements of the circulation Γ for a range of Carreau numbers Cr, corresponding to a Newtonian fluid (M9, $Cr = 0$) and all tested XG concentrations. We find that the circulation is generally enhanced as ST effects are increased. We also observe a similar trend in the vorticity magnitude both temporally and spatially for the entire cycle. At high Cr (corresponding to high

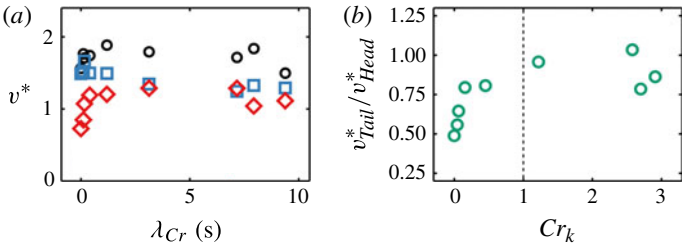

FIGURE 7. Local velocity analysis of the increase in fluid flow near the tail of the nematode. (*a*) Spatially averaged RMS-normalized fluid velocity near the head (□), midsection (○) and tail (◇) of the nematode as a function of the Carreau time scale λ_{Cr}. (*b*) The ratio of the fluid velocity at the tail to the fluid velocity at the head as a function of the kinematic Carreau number $Cr_k = \lambda_{Cr}(U/L)$.

XG concentrations), the increase in overall viscosity appears to suppress circulation: these data points are close to the power-limited regime, and for fluids above $Cr \approx 15$, the shear stresses needed to access the ST regime exceed $\sigma = 0.1$ Pa. However, for $0 < Cr < 15$ (XG concentrations $\leqslant 1000$ ppm), the measured circulation and vorticity are larger than in the Newtonian case, and this suggests agreement with previous theoretical work, which predicted enhanced vorticity in ST fluids (Vélez-Cordero & Lauga 2013).

Lastly, we quantify the decrease in fluid velocity near the head and the accompanying increase in fluid velocity near the tail observed in figures 4 and 5. In order to measure these effects, we divide the flow field region into three sections, 'head', 'mid' and 'tail'. The head section is defined as the region of the y-axis that contains the first 30 % of the worm body ($0 < s < 0.3L$) (figure 1*a*), the tail section is defined as the region that contains the last 30 % of the worm body ($0.7L < s < L$), and each section extends $0.5L$ in the positive and negative x-directions.

Figure 7(*a*) shows the normalized average velocity magnitude v^* in each region as a function of the Carreau time scale λ_{Cr}. We define v^* as $\langle v \rangle / \sqrt{\langle v^2 \rangle}$, where $\langle v \rangle$ is the local average fluid velocity in each region and $\sqrt{\langle v^2 \rangle}$ is the global RMS velocity. Increasing λ_{Cr} corresponds to increasing XG concentration, with $\lambda_{Cr} = 0$ for the M9 buffer. We find that (i) v^*_{Head} decreases slightly with increasing λ_{Cr}, (ii) v^*_{Tail} increases dramatically with increasing λ_{Cr} and plateaus at $\lambda_{Cr} \approx 3$ s, and (iii) v^*_{Mid} is largely insensitive to increasing λ_{Cr}.

To understand why ST viscosity might affect the velocity field at the head and tail differently, we consider an element of ST fluid as it passes from the head to the tail of the forward-swimming nematode. When the shear strain rate of this element changes, the characteristic time for it to approach its new steady-state viscosity is λ_{Cr} (Carreau *et al.* 1997). We therefore define a kinematic Carreau number, $Cr_k = \lambda_{Cr}(U/L)$, where U and L are the nematode's speed and length, in order to compare λ_{Cr} with the characteristic time for fluid to pass from the head to the tail. If $Cr_k \gtrsim 1$, fluid passing the tail will still be thinned from its earlier encounter with the moving head in addition to the local instantaneous body motion. However, if $Cr_k \ll 1$, the viscosity near the tail will be a function solely of the local instantaneous shear rate.

This phenomenon is made more apparent by plotting the ratio v^*_{Tail}/v^*_{Head} as a function of Cr_k. Figure 7(*b*) shows that this ratio increases monotonically with Cr_k, and becomes asymptotic near $Cr_k = 1$. These observations suggest that the velocity

of fluid near the tail is significantly enhanced when that fluid is under the influence of prior ST. Also, the variation in v^*_{Tail}/v^*_{Head} at $Cr_k \approx 3$ suggests that once again we are nearing the nematode's power-limited regime, in which the bulk viscosity seems to overwhelm ST effects. This effect of the persistence of ST, at the scale of the entire body, is qualitatively consistent with previous numerical results showing a large envelope of shear-thinned fluid along the body of a uniflagellated swimmer (Montenegro-Johnson *et al.* 2013).

6. Conclusion

We have investigated the effects of ST viscosity on the swimming kinematics and flow fields of the nematode *C. elegans* in solutions of a semi-rigid rod-like polymer (XG) in buffer solution (M9). We find no significant differences between the observed kinematics in ST fluids and the kinematics in Newtonian fluids of similar viscosity, a result consistent with recent theoretical calculations (Vélez-Cordero & Lauga 2013). Despite this experimental observation (unmodified kinematics), we find substantial differences between the resulting Newtonian and ST flow fields.

Temporal and spatial averages of the velocity fields, along with a snapshot of the flow fields at one phase in the cycle, reveal a structural difference in the flow field near the head of the worm in ST fluids when compared with the Newtonian case. The streamlines reveal that the major structural difference occurs within the dominant body vortex near the nematode's head; we quantify this effect by computing the circulation of the vortex, thereby accounting for its strength and size. We find that an increase in ST behaviour leads to an enhancement in circulation, consistent with recent theoretical calculations (see Vélez-Cordero & Lauga 2013). Furthermore, the ST flow fields reveal a decrease in average fluid velocity near the head of the organism and an increase near the tail. We find that the ratio of the average fluid velocity at the tail to that at the head increases as the Carreau time scale λ_{Cr} increases, and that this effect plateaus once λ_{Cr} is similar to the time scale of the forward swimming motion, U/L.

This experimental study systematically explores the effects of shear-thinning viscosity on the kinematics and flow fields of a model undulatory swimmer. Since numerous other biological systems, such as beating cilia, spermatozoa and bacteria, experience natural environments composed of non-Newtonian shear-thinning fluids, our findings bring us another step closer to understanding the interaction between complex fluids and low-Reynolds-number swimmers.

Acknowledgements

We thank T. Lamitina and X. Shen for their help with the experiments. This work was supported by NSF-CAREER-0954084 and by the Penn NSF MRSEC (DMR-1120901). D.A. Gagnon was supported by an NSF Graduate Research Fellowship.

References

Alexander, M. 1991 *Introduction to Soil Microbiology*. R.E. Krieger.

Brenner, S. 1974 The genetics of *Caenorhabditis elegans*. *Genetics* **77**, 71–94.

Carreau, P. J., DeKee, D. C. R. & Chhabra, R. P. 1997 *Rheology of Polymeric Systems*. Hanser.

Dasgupta, M., Liu, B., Fu, H. C., Berhanu, M., Breuer, K. S., Powers, T. R. & Kudrolli, A. 2013 Speed of a swimming sheet in Newtonian and viscoelastic fluids. *Phys. Rev.* E **87**, 013015.

FAUCI, L. J. & DILLON, R. 2006 Biofluidmechanics of reproduction. *Annu. Rev. Fluid Mech.* **38**, 371–394.

FU, H. C., SHENOY, V. B. & POWERS, T. R. 2010 Low-Reynolds-number swimming in gels. *Europhys. Lett.* **91**, 24002.

FU, H. C., WOLGEMUTH, C. W. & POWERS, T. R. 2009 Swimming speeds of filaments in nonlinearly viscoelastic fluids. *Phys. Fluids* **21**, 033102–033110.

GAGNON, D. A., SHEN, X. N. & ARRATIA, P. E. 2013 Undulatory swimming in fluids with polymer networks. *Europhys. Lett.* **104**, 14004.

GUASTO, J. S., JOHNSON, K. A. & GOLLUB, J. P. 2010 Oscillatory flows induced by microorganisms swimming in two dimensions. *Phys. Rev. Lett.* **105**, 168102.

HARMAN, M. W., DUNHAM-EMS, S. M., CAIMANO, M. J., BELPERRON, A. A., BOCKENSTEDT, L. K., FU, H. C., RADOLF, J. D. & WOLGEMUTH, C. W. 2012 The heterogenous motility of the Lyme disease spirochete in gelatin mimics dissemination through tissue. *Proc. Natl Acad. Sci. USA* **109**, 3059–3064.

LAUGA, E. 2007 Propulsion in a viscoelastic fluid. *Phys. Fluids* **19**, 083104–083113.

LAUGA, E. & GOLDSTEIN, R. E. 2012 Dance of the microswimmers. *Phys. Today* **65**, 30–35.

LAUGA, E. & POWERS, T. R. 2009 The hydrodynamics of swimming microorganisms. *Rep. Prog. Phys.* **72**, 096601.

LIU, B., POWERS, T. R. & BREUER, K. S. 2011 Force-free swimming of a model helical flagellum in viscoelastic fluids. *Proc. Natl Acad. Sci. USA* **108**, 19516–19520.

MONTENEGRO-JOHNSON, T. D., SMITH, D. J. & LOGHIN, D. 2013 Physics of rheologically enhanced propulsion: different strokes in generalized Stokes. *Phys. Fluids* **25**, 081903.

MONTENEGRO-JOHNSON, T. D., SMITH, A. A., SMITH, D. J., LOGHIN, D. & BLAKE, J. R. 2012 Modelling the fluid mechanics of cilia and flagella in reproduction and development. *Eur. Phys. J.* E **35**, 111.

PURCELL, E. M. 1977 Life at low Reynolds number. *Am. J. Phys.* **45** (1), 3–11.

RANKIN, C. H. 2002 From gene to identified neuron behavior in *Caenorhabditis elegans*. *Nat. Rev. Genet.* **3**, 622–630.

SAINTILLAN, D. & SHELLEY, M. J. 2012 Emergence of coherent structures and large-scale flows in motile suspensions. *J. R. Soc. Interface* **9**, 571–585.

SHEN, X. N. & ARRATIA, P. E. 2011 Undulatory swimming in viscoelastic fluids. *Phys. Rev. Lett.* **106**, 208101.

SZNITMAN, J., SHEN, X. N., SZNITMAN, R. & ARRATIA, P. E. 2010*a* Propulsive force measurements and flow behavior of undulatory swimmers at low Reynolds number. *Phys. Fluids* **22**, 121901.

SZNITMAN, R., GUPTA, M., HAGER, G. D., ARRATIA, P. E. & SZNITMAN, J. 2010*b* Multi-environment model estimation for motility analysis of *Caenorhabditis elegans*. *PLoS ONE* **5**, e11631.

TERAN, J., FAUCI, L. & SHELLEY, M. 2010 Viscoelastic fluid response can increase the speed and efficiency of a free swimmer. *Phys. Rev. Lett.* **104**, 038101.

VÉLEZ-CORDERO, J. N. & LAUGA, E. 2013 Waving transport and propulsion in a generalized Newtonian fluid. *J. Non-Newtonian Fluid Mech.* **199**, 37–50.

WYATT, N. B. & LIBERATORE, M. W. 2009 Rheology and viscosity scaling of the polyelectrolyte xanthan gum. *J. Appl. Polym. Sci.* **114**, 4076–4084.